Acta Materialia 237 (2022) 118145

Contents lists available at ScienceDirect

Acta Materialia

journal homepage: www.elsevier.com/locate/actamat

Full length article

Sensitive electric field control of first-order phase transition in epitaxial multiferroic heterostructures

Yao Liu[a,*], Fan Ye[b], Houbo Zhou[c], Xin Song[a], Wentao Jia[a], Andong Xiao[a], Jing Wang[c], Sheng Dai[b], Tianyu Ma[a,*], Fengxia Hu[c,d,*], Baogen Shen[c,d]

[a] Frontier Institute of Science and Technology, State Key Laboratory for Mechanical Behavior of Materials, and MOE Key Laboratory for Nonequilibrium Synthesis and Modulation of Condensed Matter, Xi'an Jiaotong University, Xian 710049, China
[b] Key Laboratory for Advanced Materials and Feringa Nobel Prize Scientist Joint Research Centre, Institute of Fine Chemicals, School of Chemistry & Molecular Engineering, East China University of Science and Technology, Shanghai 200237, China
[c] Beijing National Laboratory for Condensed Matter Physics and State Key Laboratory of Magnetism, Institute of Physics, Chinese Academy of Sciences, Beijing 100190, School of Physical Sciences, University of Chinese Academy of Sciences, Beijing 101408, China
[d] Songshan Lake Materials Laboratory, Dongguan, Guangdong 523808, China

ARTICLE INFO

Article history:
Received 20 February 2022
Revised 3 June 2022
Accepted 2 July 2022
Available online 3 July 2022

ABSTRACT

Strongly correlated electron materials that exhibit rich phase transition and multiple phase separation have shown many fascinating properties. Using these properties in the electronic device will require the ability to control their phase transition and phase separation behaviours. In this work, we report a sensitive electric field control of first-order phase transition in epitaxial (011)-$Nd_{0.5}Sr_{0.5}MnO_3$/0.71$Pb(Mg_{1/3}Nb_{2/3})O_3$–0.29$PbTiO_3$ (PMN-PT) heterostructure. The pristine film shows phase separation character with the penetration of the ferromagnetic metallic phase into the charge and orbital ordered antiferromagnetic insulating phase, and this was revealed by the XMCD and XLD investigation. The (011)-oriented PMN-PT piezoelectric single crystal adopted can exert anisotropic in-plane tensile strains on the epitaxial $Nd_{0.5}Sr_{0.5}MnO_3$ film when applying the electric field. The coaction of the electric field-induced strain and polarization effects of the PMN-PT piezoelectrics enable the efficient manipulation of orbital ordering and the coupled electronic and magnetic phase transitions. Accordingly, a small +1.6 kV cm^{-1} electric field can recover the first-order metal-insulator transition which was inhibited in the pristine heterostructure, increase the transition temperature by 56 K and the maximum resistance change reaches 7033%. Furthermore, the electric field demonstrated non-volatile control of magnetization, and the magnetoelectric coefficient reaches 1.89 × 10^{-7} s m^{-1} at 200 K. This work indicates that choosing the piezoelectric substrate with appropriate electric-field-induced strain opens a route to designing functional electronic devices where the tunable macroscopic properties derive from strongly interacting degrees of freedom present in the manganite.

1. Introduction

The strongly correlated electron materials that undergo a variety of phase transitions [1–6], including superconductivity [1,2], the metal-insulator transition [3,4], and colossal magnetoresistance [5,6] have shown great significance in science and technology. In these materials, the strong coupling between spin, lattice, and charge degrees of freedom will induce phase separation [7–10], meaning that multiple electronic/magnetic phases with diameters of nanometers to micrometers can coexist at temperatures where a pure phase is expected. Searching for approaches to control the phase transition and/or phase separation is the key to making use of the properties of those correlated electron materials in device applications [11–16].

The electric field, which is more energy-efficient than the other external field such as magnetic field and current [17–20], has shown great potential in electronic devices when it was used to tune the phase transition and the related properties in correlated electron materials. The electric field controls of resistance [21–25] and magnetism [26–30], for example, are promising in the field-effect transistor and energy-efficient magnetic storage technique. Achieving giant electric field control of resistance and magnetism is the longstanding goal, and constructing the multiferroic heterostructures by combining the correlated electron mate-

* Corresponding authors.
E-mail addresses: liuyao12@xjtu.edu.cn (Y. Liu), matianyu@xjtu.edu.cn (T. Ma), fxhu@iphy.ac.cn (F. Hu).

https://doi.org/10.1016/j.actamat.2022.118145
1359-6454/

rials with piezoelectrics is one of the potential routes [17–30]. The doped rare-earth perovskite manganites have been proven fertile in the search for both the electric field control of magnetism and resistance through the electric-field-induced strain engineering of the phase transition [25–30]. The phase transition in the manganites is always coupled with charge and orbital ordering, where the different orbital ordering configurations of the Mn^{3+} ions are accompanied by specific spin arrangements [12]. Considering that the orbital ordering couples intimately to the lattice distortion, hence, to realize sensitive electric field manipulation of phase transition in the manganites, the appropriate piezoelectrics that can introduce strain states aiming at different orbital ordering in the manganites should be selected.

$Nd_{0.5}Sr_{0.5}MnO_3$ is a fascinating rare-earth perovskite manganite [31–34]. Its defining nature is the sharp first-order phase transition from the ferromagnetic metal (FMM) to charge (Mn^{3+} and Mn^{4+} ions are alternatively arranged) and orbital (staggered $d(3x^2\text{-}r^2)$ and $d(3y^2\text{-}r^2)$ ordered insulator with the antiferromagnetic spin arrangement (COO/AFI), and multiple electronic/magnetic phases coexistence [5,12,32]. The orbital ordering plane resides in the out of the (011)-plane of $Nd_{0.5}Sr_{0.5}MnO_3$ (cubic notation) [5], as a result, the growth of (011)-oriented $Nd_{0.5}Sr_{0.5}MnO_3$ means the freedom of the orbital plane and enables the first-order metal-insulator phase transition. Moreover, the in-plane anisotropy of the orbital ordering characters means exerting anisotropic strain within the (011)-plane of $Nd_{0.5}Sr_{0.5}MnO_3$ can tune its phase transitions effectively. It was indeed revealed that the (011)-oriented $Nd_{0.5}Sr_{0.5}MnO_3$ films that underwent appropriate in-plane anisotropic strain exhibited clear first-order transition, which has not been possible in those with (001) and (111)-orientations studied extensively [33–36]. Here in this article, aiming at the manipulation of phase transition through the orbital ordering of $Nd_{0.5}Sr_{0.5}MnO_3$, we specially adopted the (011)-oriented $0.71Pb(Mg_{1/3}Nb_{2/3})O_3\text{–}0.29PbTiO_3$ (PMN-PT) single crystal with rhombohedral structure as the piezoelectric layer / substrate in the design of multiferroic heterostructure. The (011)-PMN-PT exhibits a tensile lattice strain of +0.28% for in-plane [01$\bar{1}$] and compressive strain of −0.02% for in-plane [100] directions under a small electric field of ~ ±1.6 kV cm^{-1} due to the switching of its ferroelectric domains. The coaction of the strain and polarization effects demonstrated a remarkable level of electric field control of the first-order phase transition and/or phase separation (as shown in the E – T phase diagram in Fig. 1) in the designed (011)-$Nd_{0.5}Sr_{0.5}MnO_3$/PMN-PT heterostructure. Accordingly, the giant electric field control of resistance and magnetization can be realized by a small electric field. In the heterostructure, applying a small electric field +1.6 kV cm^{-1} can recover the FMM to the COO/AFI phase transition, and increase the first-order transition temperature by 56 K, intriguing a giant resistance change of 7033% at 10 K, the values exceed the ones reported in almost all the manganite based multiferroic heterostructures [25–27,29]. The electric field also exhibited nonvolatile control of the magnetization of the films due to the coupled electronic and magnetic structures. The maximum magnetoelectric coefficient reaches 1.89×10^{-7} s m^{-1} at 200 K, and this value is comparable to the largest value reported in manganite multiferroic heterostructures. Finally, considering that the antiferromagnetic spintronics has shown great potential applications for high-density storage and high frequency, the dynamic switching on and off of the COO/AFI phase in the heterostructure also endows the multiferroic structure possible potential in the antiferromagnetic spintronics [37–40].

2. Experimental methods

$Nd_{0.5}Sr_{0.5}MnO_3$ films with a thickness of 80 nm were deposited on the (011)-oriented PMN-PT single crystal ($3 \times 5 \times 0.5$ mm^3) through the pulsed laser deposition technique. The previous studies demonstrated that the first-order phase transition occurs in the (011)-oriented films, and the film properties show no essential dependence on the thickness within 50 nm - 110 nm [34,35], and the intermediate thickness of 80 nm was thus chosen in this work. The substrates were baked at 700 °C for 1 hour in the deposition chamber. Then the films were deposited at 700 °C, in O_2 pressure of 10 Pa, and with a laser energy density of 1 J cm^{-2} operating at a pulse frequency of 2 Hz. The film thickness was controlled by the deposition time. After deposition, the films were in-situ annealed at 700 °C in O_2 pressure of 100 Pa.

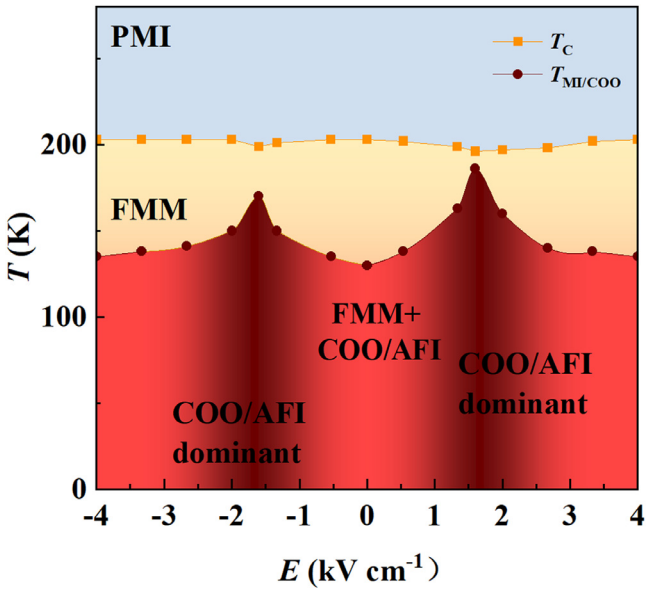

Fig. 1. The E-T phase diagram established by the transition temperatures derived from the R – T curves at various electric fields, where PMI refers to the paramagnetic insulating phase, FMM refers to the ferromagnetic metallic phase while the COO/AFI refers to charge and orbital-ordered antiferromagnetic insulating phase.

The average structure was detected using a Bruker D8 high-resolution four-circle X-ray diffraction meter, and the reciprocal maps of the (222) and (310) reflections were conducted. The X-ray absorption spectra measurement were performed at the UL beamline of the Shanghai Synchrotron Radiation Facility by tuning the synchrotron radiation at the Mn L edge, and the circular dichroism (XMCD) using the circular polarization beam and linear dichroism (XLD) by using the linear polarization beam were also measured to reveal the magnetic components in the films. The microstructure was characterized using aberration-corrected scanning transmission electron microscopy, which was performed on a ThermoFisher Themis Z microscope equipped with two aberration correctors under 300 kV. The high angle annular dark-field (HAADF)-STEM images were recorded using a convergence semi-angle of 11 mrad, and inner- and outer collection angles of 59 and 200 mrad, respectively. Cross-sectional TEM specimens were “lift-out” using the OmniProbe and thinning by a focused ion beam (FIB).

The resistance measurement under the application of electric field was conducted by a homemade holder which enables the application of electric fields by a Keithley 6517 source meter and equipped to the Quantum-design Physical Property measurement system (PPMS). The magnetic properties measurement under different electric fields was also conducted in the PPMS system by the vibrating-sample-magnetometer option. The electric field was applied by a homemade holder through a Keithley 6517 source meter. The out-of-plane lattice evolution with the electric field of the PMN-PT substrate was indirectly detected from the XRD patterns measured under cycling electric fields. The in-plane strain evolution with electric fields of the PMN-PT substrate for both the [01$\bar{1}$]

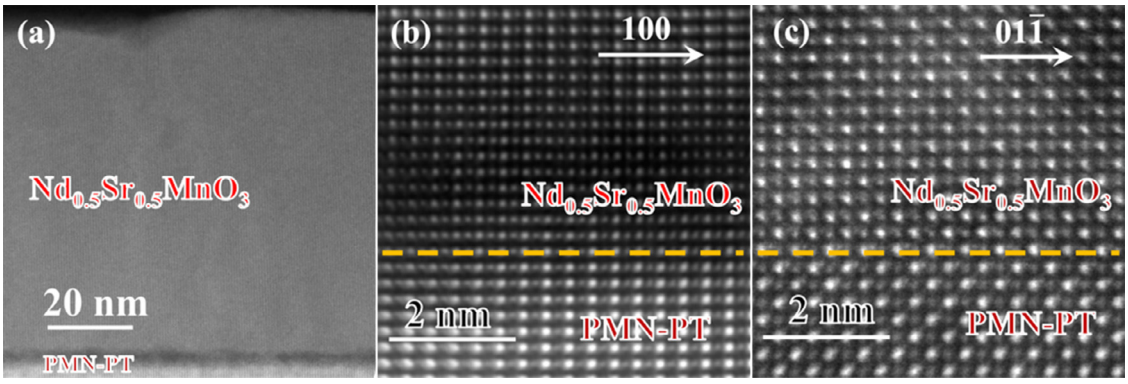

Fig. 2. The HAADF-STEM images obtained by a cs-corrected STEM from the [01$\bar{1}$] zone axis with (a) low and (b) high magnifications, and (c) from the [100] zone axis, the dotted yellow lines in (b) and (c) indicate the interface of the heterostructure.

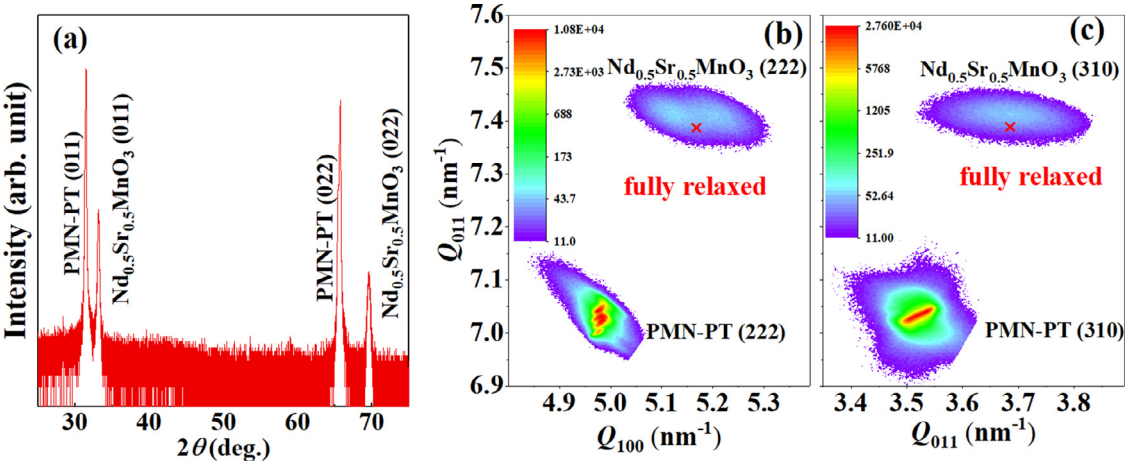

Fig. 3. (a) The 2θ-ω XRD pattern of the heterostructure. (b, c) The reciprocal map for the (222) reflections, and (310) reflections respectively, in which the cross signs indicate the positions where the film was supposed to fully relax for the [100] and [01$\bar{1}$] lattice directions.

and [100] directions was detected by the high-resolution strain gauges adhered onto the film surface.

3. Results and discussion

3.1. Structure and phase transition

The HAADF-STEM images of the heterostructure interfaces were obtained from the [01$\bar{1}$] and [100] zone axes and shown in Figs. 2(a)-(c), in which, the interfaces were marked with yellow dotted lines. The low-magnification image from [01$\bar{1}$] zone axis in Fig. 2(a) displays the homogenous morphology of the films. The epitaxial growth of the film can be confirmed from the STEM result in Figs. 2(b) and (c), and the in-plane lattice orientation relationship of $[01\bar{1}]_f$ // $[01\bar{1}]_s$ and $[100]_f$ // $[100]_s$ between the film and substrate can be identified. Bulk $Nd_{0.5}Sr_{0.5}MnO_3$ has orthorhombic symmetry with lattice parameters of a = 0.543 nm, b = 0.548 nm, and c = 0.764 nm at room temperature [41], the corresponding lattice parameters for the transferred cubic structure is $a_c = b_c$ = 3.858 Å, c_c = 3.817 Å [32]. Accordingly, the lattice mismatches (defined as $(a_f a_s)/a_s$, where a_f is the lattice parameter of the $Nd_{0.5}Sr_{0.5}MnO_3$, and a_s is the lattice parameter of the PMN-PT substrate) [42] between the film and substrate reached 3.95% for the [100] lattice, and 4.54% for the [01$\bar{1}$] lattice. This large lattice mismatch implies strain relaxation in the films with increasing thickness [42,43], which was further manifested by the investigation of the average strain state of the film. The 2θ-ω XRD pattern of the heterostructure was shown in Fig. 3(a), in which, only the (011) and (022) diffractions for the NSMO film and PMN-PT substrate manifest. RSM maps of (222) and (310) reflections were obtained and shown in Figs. 3(b) and (c). It is seen that $Nd_{0.5}Sr_{0.5}MnO_3$ film has different Q values with the PMN-PT substrate in both [100] and [01$\bar{1}$] lattices. The expected positions of the fully relaxed states for the films were marked as cross signs in Figs. 3(b) and (c). It is seen that the fully relaxed signals almost coincide with the (222) and (310) reflections of the $Nd_{0.5}Sr_{0.5}MnO_3$ film, implying that the film lattices were almost relaxed for both the in-plane [100] and [01$\bar{1}$] directions [33].

The temperature-dependent magnetization (M – T) and resistance (R – T) curves were measured to identify the phase transition of the pristine film. Following the zero-field-cooling (ZFC) M – T plot in Fig. 4(a), a paramagnetic to ferromagnetic (FM) phase transition happens with decreasing temperature (T_C = 203 K) and followed by the FM to antiferromagnetic (AFM) phase transition (T_N = 130 K), indicated by the large magnetization reduction. Below T_N, the ZFC plot and field-cooling (FC) plot split largely, and this splitting could arise from the persistence of the FM phase below T_N. For the ZFC process, the AFM phase with strong anisotropy formed and pinned the FM domains [44,45], causing zero net magnetizations at low temperatures, while for the FC process, the FM domains percolated and formed the network when the film was cooled across the T_C, thus causing higher magnetization state. The splitting thus demonstrates the persistence of the FM phase below T_N, and the depressed first-order phase transition in the pristine films.

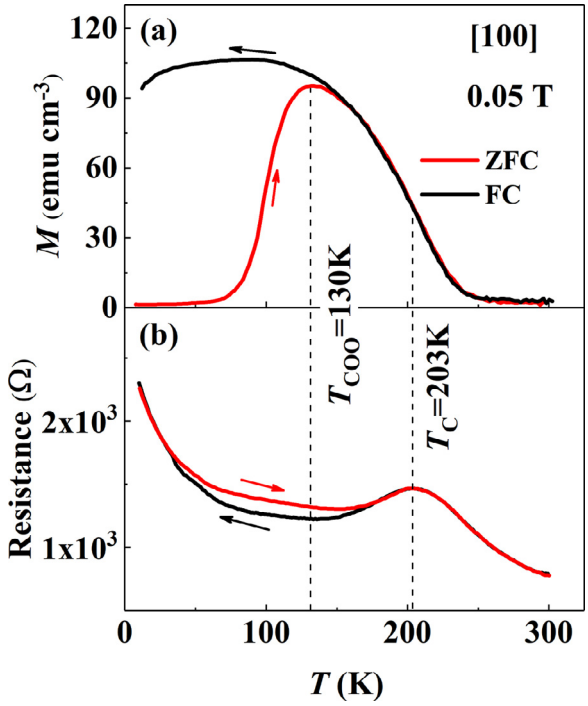

Fig. 4. (a) The M – T curves measured with zero-field-cooling and field-cooling modes in a magnetic field of 0.05 T applied along the [100] direction. (b) The R – T curves for the [100] direction under a zero magnetic field. The arrows indicate the heating and cooling process.

The R – T curves exhibited similar transition behavior with that derived from the M – T curves. The resistance increases firstly and then decreases following the cooling R – T plot, which means the insulator-metal transition and is in coincidence with the paramagnetic to ferromagnetic phase transition (T_C = 203 K). Further decreasing the temperature, the metal-insulator transition happens and the resistance enhances consistently, moreover, the cooling and heating plots of R – T curves show thermal hysteresis, implying the sign of first-order metallic to the charge and orbital ordered insulating phase transition (T_{MI} = 130 K), this transition is coupled to the FM AFM phase transition denoted in the M – T curves. Herein, we describe this transition as FMM to COO/AFI transition, and the related transition temperature T_N and T_{MI} are uniformly called $T_{MI/COO}$. It is further seen from the R – T curves that the resistance increased rather slowly below $T_{MI/COO}$, and the resistance at the low temperature was rather low, indicating that the FMM to COO phase transition was depressed in the pristine $Nd_{0.5}Sr_{0.5}MnO_3$ film [32,33]. Combining with the M – T results, it can be deduced that the slow transition and low resistance are due to the persistence of the FMM phase into the temperature where a pure COO/AFI state was expected.

Mn-XAS spectra were further recorded at the Mn-$L_{2,3}$ edge corresponding to the 2p-3d resonant transition. The spin-orbital interaction of the Mn 2p core hole splits the spectrum into two broad multiplets, the L_3 ($2p_{3/2}$) edge at lower phonon energy and the L_2 ($2p_{1/2}$) edge at higher photon energy [46]. Figs. 5(a) and (c) show the XAS spectra measured by horizontal (H) and vertical (V) polarization photons at 15 K and 180 K respectively. XLD spectra have been obtained as the difference between the two measurements (V−H) of the respective temperatures and the resulted curves are shown in respective figures. XLD is one of the few techniques that can shed light on the AFM order in films. The profound XLD signal at 15 K thus confirms the COO/AFI phase at low temperatures [47,48], and though the signal decreases in magnitude with increasing temperature, it does not disappear at 180 K, indicating the persistence of COO/AFI phase at elevated temperature, even when the temperature is above the $T_{MI/COO}$ and close to T_C, this is consistent with previous reports [48,49]. The XAS with right-handed (R) and left-handed (L) circular polarization photons were further measured and shown in Figs. 5(b) and (d), and Mn-XMCD were obtained as the difference between the two measurements (R–L). The Mn-XMCD spectra confirm the minor FM component below T_C (15 K) [48,49] and confirm the phase separation below $T_{MI/COO}$ in the pristine film further.

3.2. Electric field manipulation of phase transition and the resistance

The electric field influence on the phase transition has been characterized by the R – T curves measured under different electric fields. A certain electric field was firstly applied across the heterostructure at room temperature and then the cooling and heating plots of the resistance curves were measured under the electric field. The schematic for the measurement of resistance under electric fields was shown in Fig. 6(a). The measured R – T curves for the in-plane [100] direction under different electric fields were shown in Fig. 6(b) and (c). When an electric field of +0.5 kV cm^{-1} was applied, the $T_{MI/COO}$ increased slightly from 130 K to 138 K (inset in Fig. 6(b)), and the resistance increased compared to the 0 kV cm^{-1} curves, especially when the temperature was below the $T_{MI/COO}$. Further increasing the electric field to +1.6 kV cm^{-1}, the $T_{MI/COO}$ increased to 186 K, and the resistance below the $T_{MI/COO}$ increases tremendously, implying an almost full FMM to the COO/AFI phase transition. Otherwise, the negative electric field with the same magnitude exhibit a weaker influence on the phase transition of the heterostructures, as seen in Fig. 6(c), the transition temperature under −1.6 kV cm^{-1} increases from 130 K to 170 K. The resistance change ratio, which is defined as $(R_E\text{-}R_0)/R_0$, where R_E is the resistance value measured under an electric field of E and R_0 is the resistance value measured under 0 kV cm^{-1}, was calculated for E of +1.6 kV cm^{-1} and −1.6 kV cm^{-1} and shown in Fig. 6(d). It is seen that for +1.6 kV cm^{-1}, the change ratio reached 7033% at the lowest measuring temperature of 10 K, while for −1.6 kV cm^{-1}, the change ratio is only 478%. The magnitude of the resistance change is much higher than that reported in manganite-based multiferroic heterostructures [25-27,29], such as (111)-$La_{0.67}Ca_{0.33}MnO_3$/PMN-PT [27] and the (001)-$La_{0.5}Ca_{0.5}MnO_3$/PIN-PT [29] multiferroic heterostructures. Further increasing the applied electric field to +4 kV cm^{-1}, the resistance curves returned almost to the initial 0 kV cm^{-1} plots. Finally, when the electric field was reverted to 0 kV cm^{-1}, the R – T curves were almost identical to the initial ones.

The combined influence of magnetic field and electric field on the phase transition was further studied. The R – T curves under different magnetic fields were measured with the fixed electric field of 0 kV cm^{-1} and +1.6 kV cm^{-1} applied respectively and shown in Figs. 7(a) and (b). It is seen that the resistance decreased under the magnetic field for both 0 kV cm^{-1} and +1.6 kV cm^{-1} cases, this is because the energy gap between the COO/AFI and FMM phases is rather small in $Nd_{0.5}Sr_{0.5}MnO_3$, the magnetic field will cause the melting of the COO/AFI phase and the transition from the COO/AFI to FMM phase, which will cause the reduction of resistance and is also the origin of giant magnetoresistance in it [5]. For the pristine film, the FMM phase penetrates into temperatures where a pure COO/AFI phase was supposed, the percolation of the FMM phase thus happens under a small magnetic field, as a result, it is seen from Fig. 7(a) that the metal-insulator transition was almost fully depressed in a magnetic field 3 T. When a small electric field of +1.6 kV cm^{-1} was applied across the heterostructure (Fig. 7(b)), since the COO phase is largely stabilized by the electric field and is more robust, the first-order phase transition is thus more resistive to the magnetic field, and still distinguishable in a magnetic field as high as 7 T. This fact can be seen in Fig. 7(c),

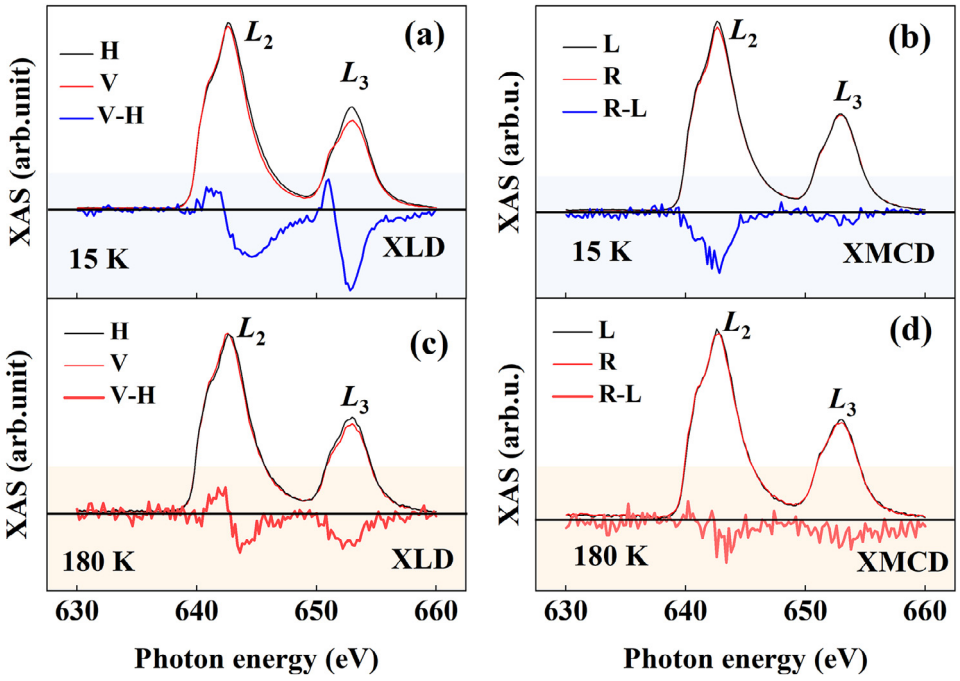

Fig. 5. (a, c) The XAS spectra obtained by the horizontal (H) and vertical (V) polarization and the obtained XLD (V−H) spectra at 15 K and 180 K respectively. (b, d) The XAS spectra obtained by the right-circle (R) and left-circle (L) polarizations and the obtained XMCD (R−L) spectra at 15 K and 180 K respectively.

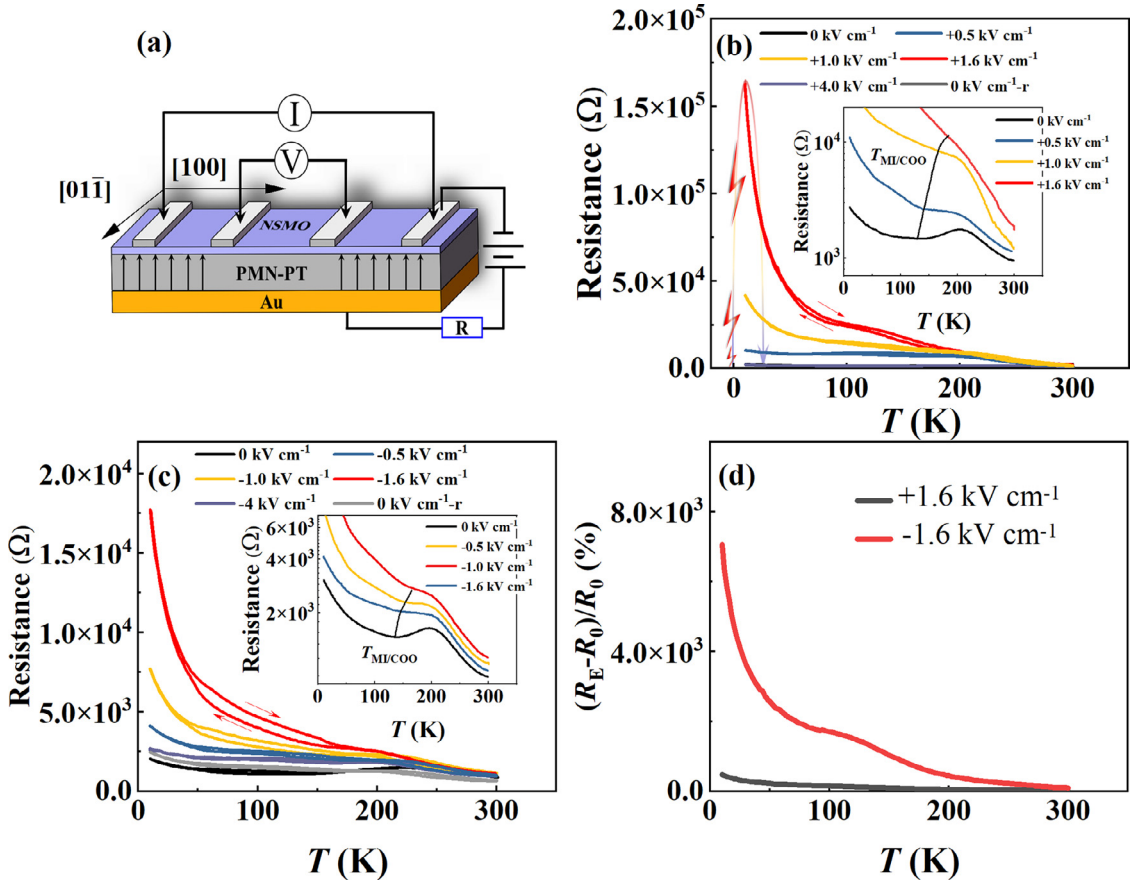

Fig. 6. (a) The schematic for the measurement of resistance under an electric field in the heterostructures. (b) The R – T curves under various electric fields applied, (c) The R – T curves under various negative electric fields, and (d) the resistance changes ratio evolution with temperatures for the E of +1.6 kV cm^{-1} and −1.6 kV cm^{-1} cases. The insets in (b) and (c) show the magnified R-T regions where the character transition temperatures can be observed.

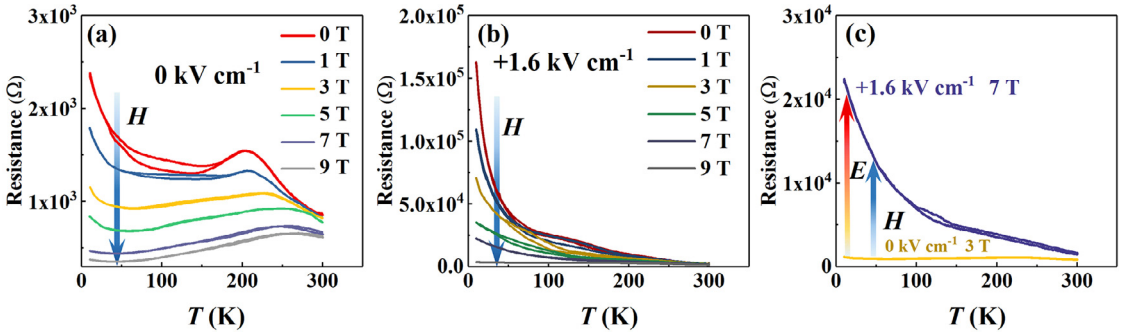

Fig. 7. (a) The $R - T$ curves were measured under different magnetic fields from 0 T to 9 T in the absence of an electric field. (b) The $R - T$ curves under different magnetic fields from 0 T to 9 T with the +1.6 kV cm^{-1} electric field applied. (c) The detailed comparison between the $R - T$ curves measured under the combined applications magnetic field and electric field of 3 T and 0 kV cm^{-1}, and +1.6 kV cm^{-1} and 7 T.

in which the $R - T$ curves at 0 kV cm^{-1}, 3 T, and +1.6 kV cm^{-1}, 7 T were shown together.

From the resistance measurements, it can be deduced that the application of proper electric fields can tremendously intrigue the metal-insulator transition in $Nd_{0.5}Sr_{0.5}MnO_3$ film, and increase the first-order FMM to COO/AFI transition temperature $T_{MI/COO}$ by 56 K. After withdrawing the electric field, the phase transition behavior can recover almost to the initial one where the FMM phase percolated in the COO/AFI phase. The results demonstrate that the electric field can dynamically switch the COO/AFI phase on and off, and the COO/AFI phase is more resistive to the external magnetic field.

3.3. Electric field manipulation of magnetism in $Nd_{0.5}Sr_{0.5}MnO_3$/PMN-PT heterostructures

As aforementioned, the spin, charge, and orbital degrees of the order are intimately coupled in $Nd_{0.5}Sr_{0.5}MnO_3$, due to which, the metallic phase has linear FM spin configuration, while the COO phase has CE type antiferromagnetic spin configuration. Hence, it can be reasonably deduced that the heterostructure would exhibit a converse magnetoelectric (ME) effect. Investigating the converse ME effect not only explores the application possibility of the heterostructure in the magnetic storage technique, but also promotes the understanding of the electric field control of phase transition. The electric field manipulation of magnetization in the heterostructures was thus studied further.

The sample was firstly zero-field-cooled to target temperatures of 200 K, 150 K, and 100 K respectively, and the magnetization loops were measured with subsequently applied electric fields of 0 kV cm^{-1}, +6 kV cm^{-1} and after withdrawing +6 kV cm^{-1} (0 kV cm^{-1}-r). The measured magnetization curves for the [01$\bar{1}$] and [100] directions are shown in Fig. 8. Comparing the magnetization loops along the [01$\bar{1}$] and [100] directions, the magnetization shows magnetic anisotropy, with the [100] axis being the easy magnetic direction and the [01$\bar{1}$] axis being the hard magnetic direction. The electric field displays a great influence on the magnetization loops of the film, while minor influence on the coercivity or magnetic anisotropy of the heterostructures. At 200 K (Fig. 8(a) and (b)), it is seen that the magnetization at the maximum magnetic field at 1 T decreases when applying +6 kV cm^{-1} electric field for both [100] and [01$\bar{1}$] directions, and with the temperatures decreasing to 150 K (Fig. 8(c) and (d)) and 100 K (Fig. 8(e) and (f)), the electric field influence on the magnetization loops weakens.

The magnetization evolution with the electric field ($M - E$ curves) was further measured in a magnetic field of 0.05 T. The measured $M - E$ curves for both the [100] and [01$\bar{1}$] at the respective temperatures are shown in Figs. 9(a)-(h). It is seen that the magnetization along both the in-plane [100] and [01$\bar{1}$] directions exhibited similar responses to the applied electric field at all measurement temperatures. At 250 K, well above the T_C, the $M - E$ curves display butterfly shape (Figs. 9(a) and (b)), the magnetization reduces and then recovers to the initial states when the electric field increases from 0 kV cm^{-1} to +6 kV cm^{-1}. At 200 K, the $M - E$ curves show loop-like shapes (Figs. 9(c) and (d)), and the magnetization decreases continuously by 41.5 emu cm^{-3} with the electric field up to +6 kV cm^{-1}. The reduction ratio which is defined as $(M_E - M_0)/M_0$, where M_E is the magnetization value at electric field E and M_0 is the magnetization value at 0 kV cm^{-1}, reached 32.5% for the electric field of +6 kV cm^{-1}. Moreover, the lower magnetization state at +6 kV cm^{-1} is almost retained when the electric field was withdrawn to 0 kV cm^{-1}, and only reversing the electric field to −6 kV cm^{-1} will recover the magnetization to the initial state. The electric field manipulation of magnetization thus shows a non-volatile memory effect at 200 K. The nonvolatile control of magnetism was highly desirable in the magnetic storage technique since it means that the pulsed electric fields can stimulate two or more magnetization states [50,51]. For the present multiferroic heterostructures, it is seen from Fig. 10(a) that the low and high magnetization states can be induced by + 6 kVcm^{-1} and −6 kV cm^{-1} pulsed electric field, and the magnetization states induced by the pulsed electric field shows good retention after more than fifty cycles. Moreover, the maximum magnetoelectric coefficient ($\alpha_{ME} = u_0 dM/dE$) accompanying the evolution of electric fields at 200 K can reach 1.89 × 10^{-7} s m^{-1} as is shown in Fig. 10(b). The value is larger than that obtained in most manganite based multiferroic heterostructures, such as the (001)-$Pr_{0.3}Sr_{0.7}MnO_3$/PMN-PT [28] and the (111)-$La_{0.5}Ca_{0.5}MnO_3$/PIN-PT [29] et al., and is comparable to the values reported in the $La_{0.67}Sr_{0.33}MO_3/BaTiO_3$, which possessed the largest ME coefficient value in the manganite based heterostructures up to now [50]. However, the value is still lower than the ones in the FeRh/$BaTiO_3$ (1.6 × 10^{-5} s m^{-1}) [52]. When further reducing the temperature to 150 K (Figs. 9(e) and (f)), it is seen the $M - E$ curves have a similar shape to that at 200 K, the difference is that the magnitude of magnetization changes with the electric field decreased. The magnetization reduction is 16.0 emu cm^{-3} and the change ratio is 9.7% for electric field change from 0 to +6 kV cm^{-1}. Finally, at 100 K (Figs. 9(g) and (h)), the electric field influence on magnetization almost disappeared.

3.4. Revisiting the electric field-induced strain in the (011)-oriented PMN-PT

The electric field-induced ferroelectric domain switching and the accompanying lattice strain in the present PMN-PT piezoelectric were thus studied further to unveil the strain mediation of the phase transition in the present heterostructures. The lattice strain for the out-of-plane [011] direction has been studied by the (022)-

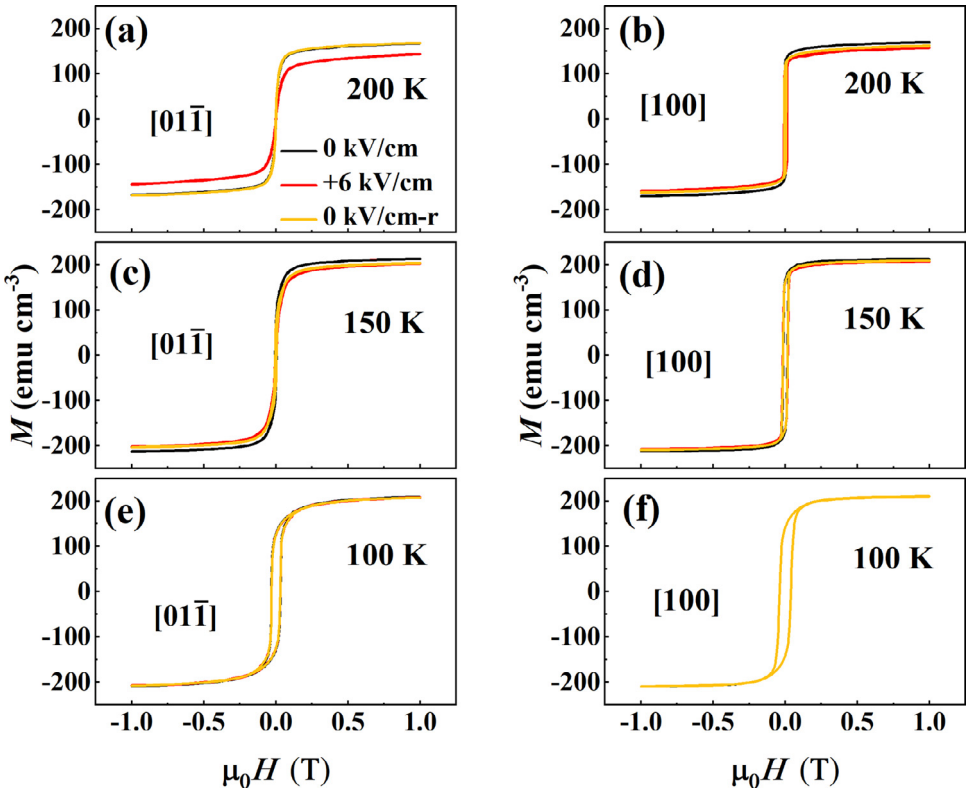

Fig. 8. Magnetization loops measured at various temperatures of (a, b) 200 K, (c, d) 150 K, (e, f) 100 K in [01$\bar{1}$] and [100] lattice directions respectively. The sample was cooled in zero magnetic field and electric field to the target temperatures, then the magnetization loops were measured with the electric field of 0 kV cm^{-1}, +6 kV cm$^{-1,}$ and withdrawing the +6 kV cm^{-1} electric field (0 kV cm^{-1}-r).

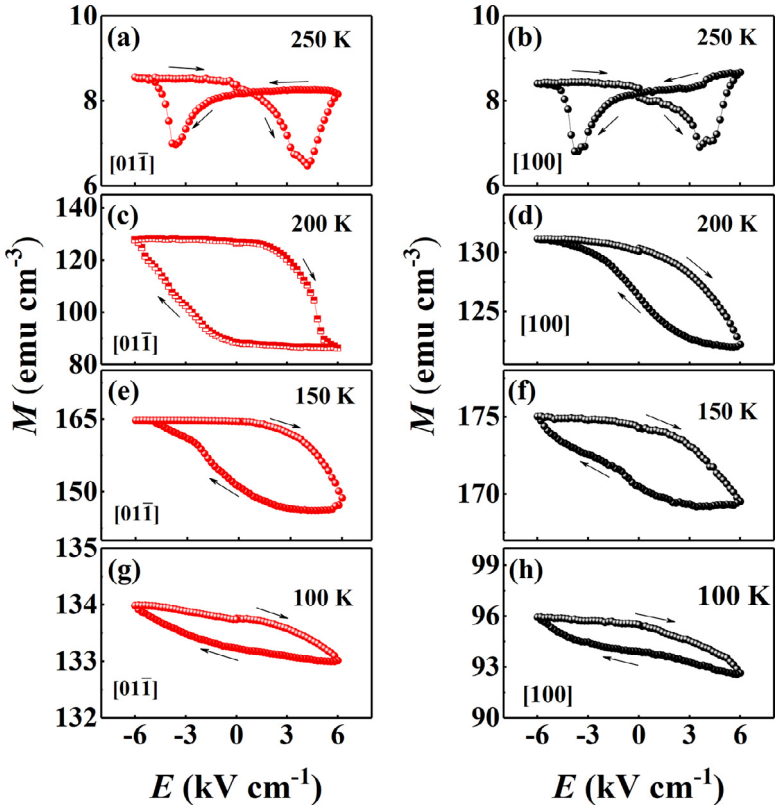

Fig. 9. Magnetization evolution with electric field curves measured at various temperatures of (a, b) 250 K, (c, d) 200 K, (e, f) 150 K, and (g, h) 100 K in [01$\bar{1}$] and [100] lattice directions respectively. The sample was cooled in zero magnetic field and electric field to the target temperatures, subsequently, a magnetic field of 0.05 T was applied and followed by measuring the $M - E$ curves.

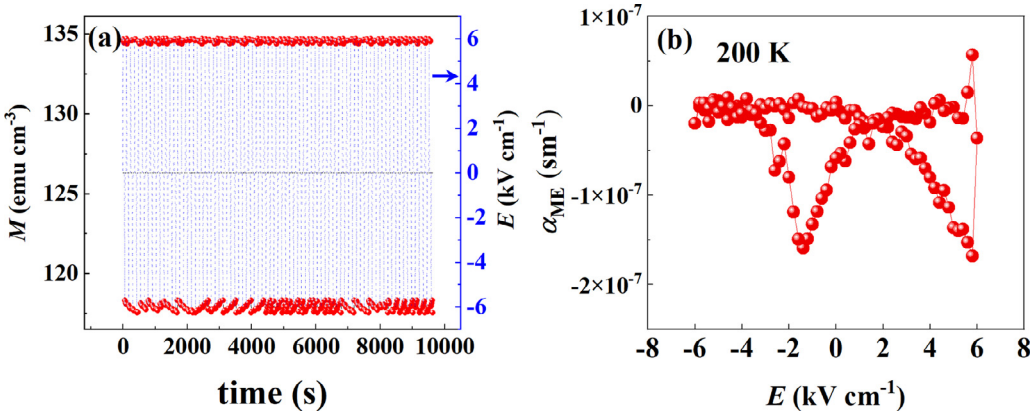

Fig. 10. (a) The high and low magnetization states induced by +6 kV cm^{-1} and −6 kV cm^{-1} pulsed electric field in the heterostructure at 200 K and magnetic field of 0.05 T. (b) The magneto-electric coefficient obtained by $u_0 dM/dE$ using the $M - E$ curves at 200 K.

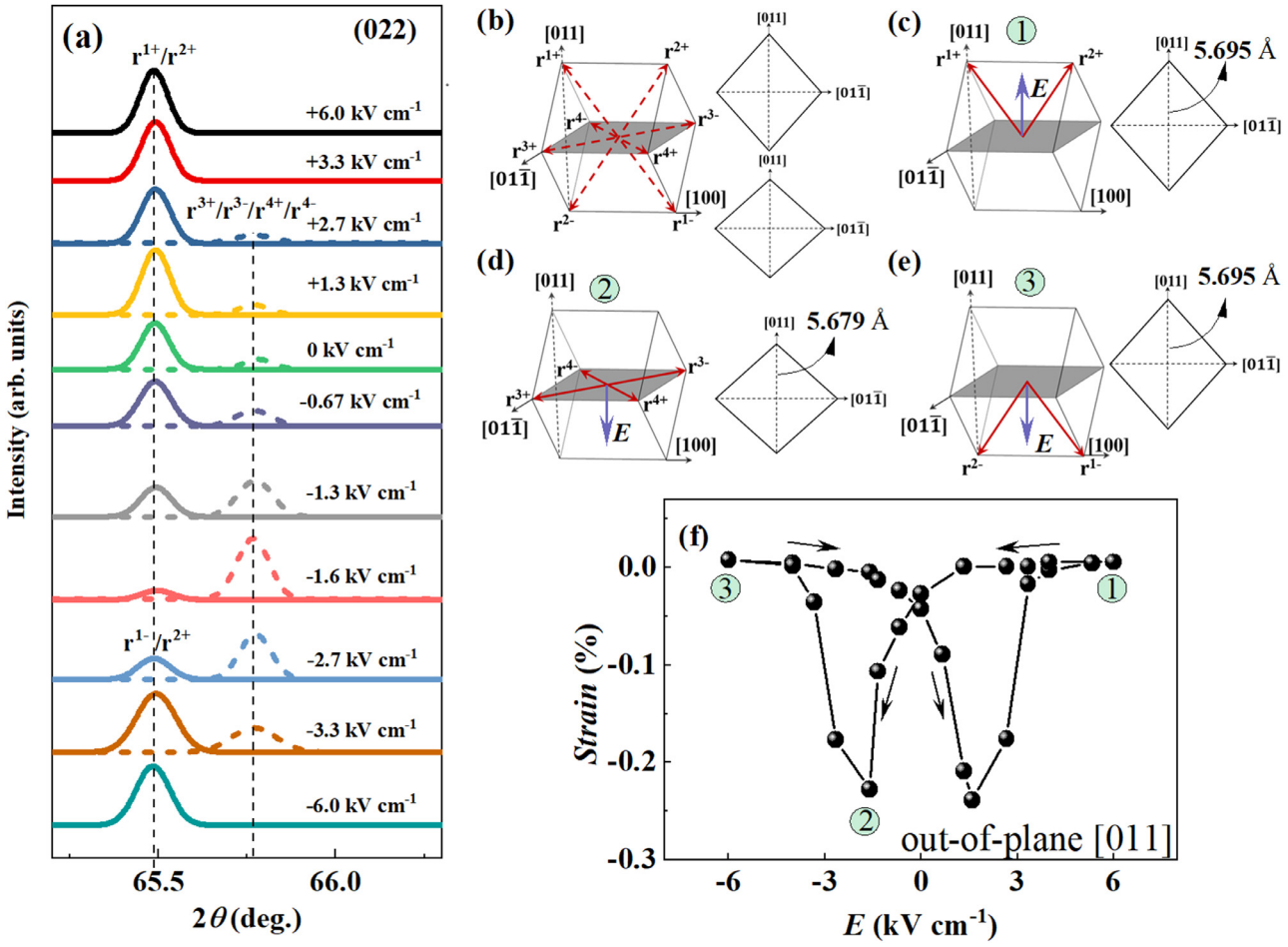

Fig. 11. (a) The XRD patterns with (022)-peaks measured under different electric fields from –6 kV cm^{-1} to +6 kV cm^{-1} at room temperature, the electric field was applied across the out-of-plane ⟨011⟩ direction. (b) The schematic for the polarization states of the unpoled PMN-PT substrate, (c) poled with the electric field of +6 kV cm^{-1}, (d) poled with an electric field of −1.6 kV cm^{-1}, (e) poled with an electric field of −6 kV cm^{-1}. (f) The strain versus electric field curve at room temperature for the out-of-plane [011] direction. The arrows in the figure indicate the evolution of the electric fields.

peaks in the XRD patterns conducted at different electric fields, as shown in Fig. 11(a). PMN-PT has a rhombohedral structure with $a = 4.017$ Å and $\alpha = 89.9°$ at room temperature [53], with the ferroelectric polarizations pointing to ⟨111⟩ directions of the pseudo-cubic cell [54], as shown in Fig. 11(b). When the PMN-PT was poled by an upward +6 kV cm^{-1} electric field along the out-of-plane ⟨011⟩ direction, the polarizations were switched to r^{1+}/r^{2+} (Fig. 11(c)), and can be confirmed from the (022)-peak of the PMN-PT measured with +6 kV cm^{-1} electric field, in which, only one diffraction peak residing at 65.50° can be identified. When reversing the electric field direction and reducing the positive electric field, another diffraction peak residing at 65.75° appears. This is in accordance with the 71° and 109° polarization switching from r^{1+}/r^{2+} to $r^{3+}/r^{3-}/r^{4+}/r^{4-}$[53]. Further reversing the electric field downward, at −1.6 kV cm^{-1}, the peak corresponding to $r^{3+}/r^{3-}/r^{4+}/r^{4-}$ polarization dominates (Fig. 11(d)). In this pro-

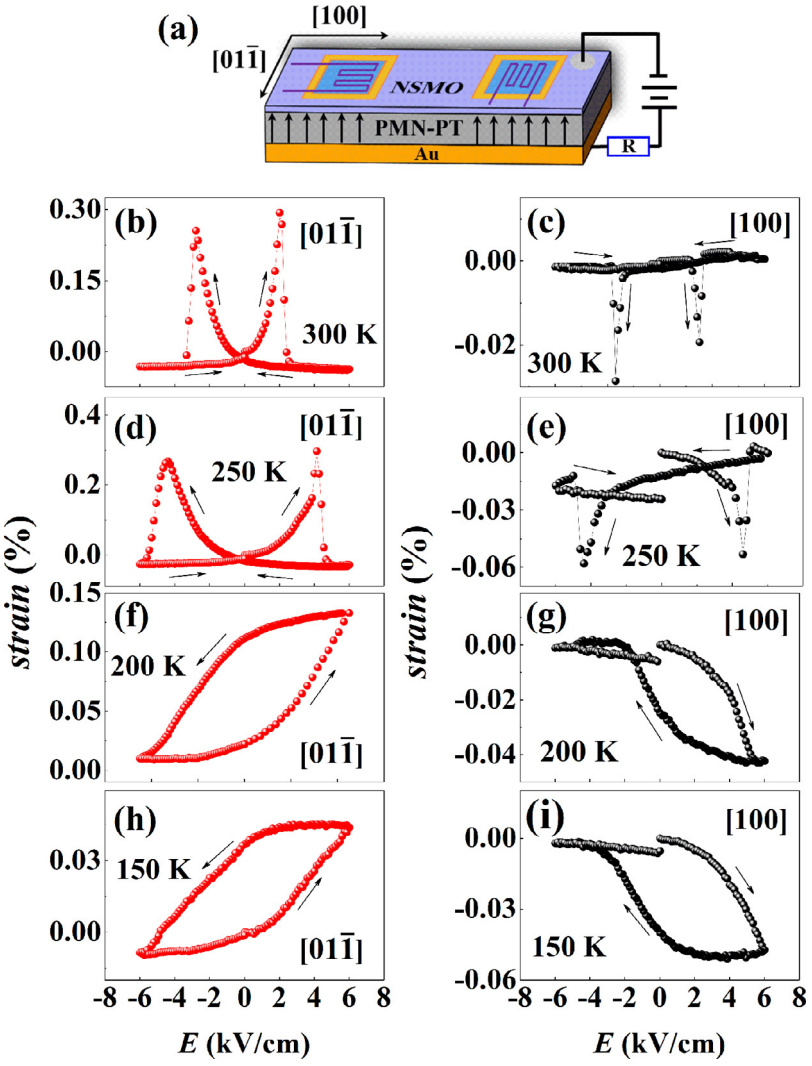

Fig. 12. (a) The schematic for the measurement of the in-plane strain curves by high-resolution strain gage adhered to the sample. Strain evolution with the electric field at temperatures of (b, c) 250 K, (d, e) 200 K, (f, g) 150 K, and (h, i) 100 K for the in-plane [100] and [01$\bar{1}$] directions respectively. The arrows indicate the cycling of electric fields.

cess, strong compressive strain along the [011] direction arises from the difference in the *d*-spacing between the r^{1+}/r^{2+} and $r^{3+}/r^{3-}/r^{4+}/r^{4-}$ polarizations, as shown in Figs. 11(c) and (d). Further increasing the negative electric field, the polarization switches to r^{1-}/r^{2-} (Fig. 11(e)), the (022) diffraction peak converts to the mere one residing at 65.50°, the strain value decreased during this process and reverted to the +6 kV cm^{-1} state. The polarization process from −6 kV cm^{-1} to +6 kV cm^{-1} was almost symmetric with the one from +6 kV cm^{-1} to −6 kV cm^{-1}, and the strain curves possess butterfly shape. The out-of-plane lattice strain corresponding to the polarization switching was calculated through the (022)-peak shift and shown in Fig. 11(f).

The in-plane strain evolution with electric field measurement was also measured by strain gauges adhered onto the film surface, the schematic for the measurements was shown in Fig. 12(a). The strain evolution for the room temperature case is consistent with the polarization switching process demonstrated in Fig. 11. As shown in Figs. 12(b) and (c), the strain – *E* curves at room temperature also exhibited butterfly shape for in-plane [01$\bar{1}$] and [100] directions. As shown in Fig. 11(c)-(f), the compressive strain for the out-of-plane direction is coupled with a tensile strain of +0.28% at ~ +1.6 kV cm^{-1} for the [01$\bar{1}$] direction. The in-plane [100] lattice exhibited a minor compressive strain of –0.02%, demonstrating that the lattice parameter (*a*) change during the polarization process is negligible. The in-plane strain – *E* curves were also measured at low temperatures of 250 K, 200 K, 150 K, and 100 K. At 250 K (Figs. 12(d) and (e)), the curves showed a similar butterfly shape to that at 300 K, with the maximum strain value occurring at ~ ±4.2 kV cm^{-1}, indicating the polarization switching field is larger than the ones at room temperature. Further decreasing temperature to 200 K (Figs. 12(f) and (g)), the strain curves exhibited a loop-like shape. These behaviors were caused by the enhancement of coercivity of PMN-PT at lower temperatures [54,55]. Since the strain occurs by small displacement of atoms in the piezoelectric [54,55], when the temperature is decreased, a higher electric field is required to reverse the atomic displacement due to the reduced thermal agitation [55]. Consequently, at 200 K, the +6 kV cm^{-1} electric field cannot fully polarize the randomly distributed polarizations to r^{1+}/ r^{2+}, and can only switch the polarization to $r^{3+}/r^{3-}/r^{4+}/r^{4-}$, at this state, reversing the electric field, the $r^{3+}/r^{3-}/r^{4+}/r^{4-}$ polarizations retained at 0 kV cm^{-1}, and cause the remnant strain state, further decreasing electric field to –6 kV cm^{-1}, the $r^{3+}/r^{3-}/r^{4+}/r^{4-}$ polarizations partially switched to the r^{1-}/r^{2-}, the strain state reverted to the initial state and caused loop-like shape. As a result, the strain – *E* curve exhibited a loop-like shape and reduced strain values at 200 K. Further lowering the

temperature, for example, 100 K (Figs. 12(h) and (i)), the maximum electric field of +6 kV cm^{-1} can hardly switch the polarization and the strain reduces further.

3.5. Mechanism of the electric field control of phase transition

Combining the resistance, magnetization, and strain measurement under electric field, the characters of the electric field control of resistance and magnetization behavior can be summarized as follows: i) applying an appropriate electric field at room temperature will enforce the first-order phase transition and enhance the resistance, and the positive and negative electric fields with the same absolute magnitude exert asymmetric influence on the resistance curves. ii) the M – E and strain – E curves at respective temperatures showed quite similar shapes. iii) The electric field showed a similar influence on the magnetization for the in-plane [100] and [01$\bar{1}$] directions while weak influence on the coercivity or magnetic anisotropy. All these demonstrate that the electric field control of magnetism and resistance was through the coaction of strain and the polarization effects that manipulate the FM metallic to COO AFI phase transition in the film. In the following, we will discuss the electric field control of phase transition in the heterostructure.

As aforementioned, the negligible lattice strain depressed the COO/AFI phase transition in the pristine $Nd_{0.5}Sr_{0.5}MnO_3$ film. Under this state, applying electric fields at room temperature means dynamically applying anisotropic strain to the almost relaxed $Nd_{0.5}Sr_{0.5}MnO_3$ film. The charge-ordered insulating phase is accompanied by the orbital ordering and CE-type antiferromagnetic spin configuration [5,8,12]. In which, the orbital ordering couples intimately to the lattice distortion, and one can easily envision that the anisotropic strain will facilitate the $d(3x^2\text{-}r^2)/d(3y^2\text{-}r^2)$ orbital configuration [32–34]. The electric field (+1.6 kV cm^{-1}) induced in-plane anisotropic strain (with the tensile strain of ~ +0.28% in [01$\bar{1}$] direction, and −0.02% compressive strain in [100] direction) will enhance the orthorhombicity, deepen Jahn-Teller distortion and MnO_6 octahedral distortion, and stabilize the orbital configuration of $d(3x^2\text{-}r^2)/d(3y^2\text{-}r^2)$, the charge-ordered insulating and AFM phase coupled to the orbital ordering was thus stabilized by the pre-applied stress. Furthermore, the anisotropic deepen Jahn-Teller distortion will also localize the e_g d-electrons of the Mn^{3+} ions and stabilize the insulating state. As a result, the pre-applied stress by the electric field at room temperature will facilitate the COO/AFI phase transition, which was manifested in the R – T curves. The present results clearly denote that the electric field manipulation of the phase transition is intimately related to the electric field-induced strain state. When further increasing the electric field to +4 kV cm^{-1}, the strain state is almost identical to the 0 kV cm^{-1} case, the phase transition behavior is almost the same as that of the initial ones. Furthermore, when withdrawing the electric field to 0 kV cm^{-1}, the strain state reverts to the initial state, and the phase transition also reverts to the initial one consistently.

If only the electric field-induced strain effect is considered, the asymmetric electric field control of resistance curves by the negative and positive electric fields cannot be explained. It should be noted that the electric field cannot only induce the piezoelectric effect but also polarize the $Nd_{0.5}Sr_{0.5}MnO_3$ [30,56,57]. In the present heterostructures, applying a positive electric field across the heterostructure will cause a depletion of holes and an accumulation of electrons at the interface. Considering the coupling of the COO phase transition with the charging order of degree, the accumulation of electrons will stabilize the COO phase according to the phase diagram of $Nd_{1-x}Sr_xMnO_3$[12], on the contrary, the accumulation of the holes at the interface under negative polarization will destabilize the COO phase and cause the reduction of resistance. However, the total resistance still increases under negative polarization because the strain effect plays a major role. In addition, there is another factor that should be considered, that is, the cracks of PMN-PT due to the microscopic internal stress produced at domain boundaries by electrostriction and domain switching deformations under cyclic electric fields [58,59]. In the intermetallic-based multiferroic heterostructures, for example, the MnPt/PMN-PT [58] and $Fe_{85}Mn_{15}$/PMN-PT [59] heterostructures, since the intermetallic is ductile, the reversible cracks under the cycled electric field induce non-volatile colossal electroresistance/magnetoelectric effect [58,59]. The present $Nd_{0.5}Sr_{0.5}MnO_3$ ceramics and is hard and brittle and the electric field-induced cracks cannot be closed by the cycling of the electric field, which means that if the large resistance states was induced by the electric field-induced cracks effect, then the resistance state cannot be recovered by cycling the electric field. However, our results show that the resistance curves can recover almost to the initial ones, the crack influence was thus ruled out in the present case.

For the electric field control of magnetization, at 250 K, the butterfly-shaped strain curves result in the butterfly-shaped M – E curves, with the maximum magnetization reduction happening at the electric field which produces a maximum anisotropic strain. Further lowering the temperature to 200 K, applying +6 kV cm^{-1} caused +0.11% tensile strain for the [01$\bar{1}$] direction while −0.04% compressive strain along the [100] direction. This anisotropic tensile strain will facilitate the COO/AFI phase and change the phase separation scenario of the film, enhancing the COO/AFI phase ratio and reducing the magnetization accordingly. Obviously, the non-volatile control of magnetization at this temperature originates from the memory effect of the strain. Further decreasing the temperature, the magnitude of strain decreases greatly, and the electric field effect on the magnetization weakens consistently. It is worthy to mention that the electric field control of phase separation characters persists into temperatures higher than $T_{MI/COO}$, saying 200 K, where the film was supposed to get into the ferromagnetic state. Usually, the electric field control of magnetization of a pure ferromagnetic state should be through the manipulation of magnetocrystalline anisotropy, in which the tensile lattice strain will increase the magnetization while the compressive lattice strain will decrease the magnetization [60–62]. This can be explained by the XLD results, which demonstrated that the COO/AFM phase persisted to temperatures higher than $T_{MI/COO}$, as a result, the electric field control of phase separation dominates within a wide temperature range in $Nd_{0.5}Sr_{0.5}MnO_3$.

4. Conclusions

Both electric field control of magnetism and resistance has been realized in $Nd_{0.5}Sr_{0.5}MnO_3$/PMN-PT multiferroic heterostructure. Aiming at the orbital ordering configuration in $Nd_{0.5}Sr_{0.5}MnO_3$, and combing the coupling nature between the lattice and orbital, the (011)-PMN-PT single crystalline piezoelectric which can produce appropriate anisotropic strain was chosen as the substrate. The coaction of the electric field-induced anisotropic strain and the polarization effect can effectively tune the first-order phase transition and phase separation characters of the film. As a result, the application of ~ + 1.6 kV cm^{-1} electric field at room temperature can recover the first-order phase transition that is almost absent in the pristine film, and induce a resistance change of 7033%, demonstrating a sensitive electric field control of phase transition. In the meanwhile, the electric field can influence the phase separation scenario between the FMM and COO/AFI phases in the film, and demonstrate the manipulation of magnetization, the magnetoelectric coefficient can reach 1.89 × 10^{-7} s m^{-1}, the value is comparable to the largest values reported in the manganite based heterostructures. Moreover, the electric field manifested a nonvolatile control of magnetization due to the strain memory effect of PMN-

PT. Our results suggest that strain engineering of the orbital ordering configuration which is coupled to the lattice distortion provides a powerful approach to tune the phase transition and phase separation in the correlated electron materials. This opens a route to design functional electronic devices where the tunable macroscopic properties derive from strongly interacting degrees of freedom present in the manganite.

Declaration of Competing Interest

The authors declare that they have no known competing financial interests or personal relationships that could have appeared to influence the work reported in this paper.

Acknowledgments

This work was supported by the National Natural Science Foundation of China (Nos. 51901170, 52088101, U1832219, 51971240). The fund of the State Key Laboratory of Solidification Processing in NPU (Grant No. SKLSP202003). The Fundamental Research Funds for the Central Universities, and Shanghai Rising-star Program (20QA1402400). The National Key Research and Development Program of China (Nos. 2021YFB3501401, 2021YFB3501202, 2020YFA0711502, 2019YFA0704900). The Key Program and Strategic Priority Research Program (B, XDB33030200) of the Chinese Academy of Sciences. The authors acknowledge Beamline BL08U1A in Shanghai Synchrotron Radiation Facility (SSRF) for XAS measurements, and Instrument & Analysis Center of XJTU for experimental assistance.

References

[1] G. Campi, A. Bianconi, N. Poccia, G. Bianconi, L. Barba, G. Arrighetti, D. Innocenti, J. Karpinski, N.D. Zhigadlo, S.M. Kazakov, M. Burghammer, M. Zimmermann, M. Sprung, A. Ricci, Inhomogeneity of charge-density-wave order and quenched disorder in a high-Tc superconductor, Nature 525 (2015) 359–362.
[2] A. Bianconi, N. Poccia, Superstripes and complexity in high-temperature superconductors, J. Supercond. Nov. Magn. 25 (2012) 1403.
[3] K.H. Ahn, T. Lookman, A.R. Bishop, Strain-induced metal-insulator phase coexistence in perovskite manganites, Nature 428 (2004) 401–404.
[4] M. Fäth, S. Freisem, A.A. Menovsky, Y. Tomioka, J. Aarts, J.A. Mydosh, Spatially inhomogeneous metal-insulator transition in doped manganites, Science 285 (1999) 1540–1542.
[5] H. Kuwahara, Y. Tomioka, A. Asamitsu, Y. Moritomo, Y. Tokura, A first-order phase transition induced by a magnetic field, Science 270 (1995) 961–963.
[6] Y. Murakami, J.J. Kasai, H. Kim, S. Mamishin, D. Shindo, S. Mori, A. Tonomura, Ferromagnetic domain nucleation and growth in colossal magnetoresistive manganite, Nat. Nanotechnol. 5 (2010) 37–41.
[7] C. Ortix, J. Lorenzana, C. Di Castro, Coarse grained models in coulomb frustrated phase separation, J. Phys: Condens. Matter 20 (2008) 434229.
[8] A. Moreo, S. Yunoki, E. Dagotto, Phase separation scenario for manganese oxides and related materials, Science 283 (1999) 2034–2040.
[9] E. Dagotto, Complexity in strongly correlated electronic systems, Science 309 (2005) 257–265.
[10] C. Renner, G. Aeppli, B.G. Kim, Y.A. Soh, S.W. Cheong, Atomic-scale images of charge ordering in a mixed-valence manganite, Nature 416 (2002) 518–521.
[11] W.G. Wei, Y.Y. Zhu, Y. Bai, H. Liu, K. Du, K. Zhang, Y.F. Kou, J. Shao, W.B. Wang, D.L. Hou, S. Dong, L.F. Yin, J. Shen, Direct observation of current-induced conductive path in colossal-electroresistance manganite thin films, Phys. Rev. B 93 (2016) 035111.
[12] R. Kajimoto, H. Yoshizawa, H. Kawano, H. Kuwahara, Y. Tokura, K. Ohoyama, M. Ohashi, Hole-concentration-induced transformation of the magnetic and orbital structures in $Nd_{1-x}Sr_xMnO_3$, Phys. Rev. B 60 (1999) 9506.
[13] R.W. Li, H.B. Wang, X.W. Wang, X.Z. Yu, Y. Matsuib, Z.H. Cheng, B.G. Shen, E.W. Plummere, J.D. Zhang, Anomalously large anisotropic magnetoresistance in a perovskite manganite, PNAS 106 (2009) 14224–14229.
[14] T.Z. Ward, J.D. Budai, Z. Gai, J.Z. Tischler, L.F. Yin, J. Shen, Elastically driven anisotropic percolation in electronic phase-separated manganites, Nat. Phys. 5 (2009) 885–888.
[15] J.D. Zhang, X.L. Tan, M.K. Liu, S.W. Teitelbaum, K.W. Post, F. Jin, K.A. Nelson, D.N. Basov, W.B. Wu, R.D. Averitt, Cooperative photoinduced metastable phase control in strained manganite films, Nat. Mater. 15 (2016) 956–961.
[16] M. Jiang, X.Z. Chen, X.J. Zhou, B. Cui, Y.N. Yan, H.Q. Wu, F. Pan, C. Song, Electrochemical control of the phase transition of ultrathin FeRh films, Appl. Phys. Lett. 101 (2012) 172906.
[17] W. Eerenstein, N.D. Mathur, J.F. Scott, Multiferroic and magnetic materials, Nature 442 (2006) 759–765.
[18] J. Ma, J.M. Hu, Z. Li, C.W. Nan, Recent progress in multiferroic magnetoelectric composites: from bulk to thin films, Adv. Mater. 23 (2011) 1062–1087.
[19] Z.X. Feng, H. Yan, Z.Q. Liu, Electric-field control of magnetic order: from FeRh to topological antiferromagnetic spintronics, Adv. Electron. Mater. 5 (2019) 1800466.
[20] L.W. Martin, R. Ramesh, Multiferroic and magnetoelectric heterostructures, Acta Mater 60 (2012) 2449–2470.
[21] N.B. Aetukuri, A.X. Gray, M. Drouard, M. Cossale, L. Gao, A.H. Reid, R. Kukreja, H. Ohldag, C.A. Jenkins, E. Arenholz, K.P. Roche, H.A. Dürr, M.G. Samant, S.S.P. Parkin, Control of the metal-insulator transition in vanadium dioxide by modifying orbital occupancy, Nat. Phys. 9 (2013) 661–666.
[22] R. Scherwitzl, P. Zubko, I.G. Lezama, S. Ono, A.F. Morpurgo, G. Catalan, J.M. Triscone, Electric-field control of the metal-insulator transition in ultrathin $NdNiO_3$ films, Adv. Mater. 22 (2010) 5517–5520.
[23] B. Kundys, V. Iurchuk, C. Meny, H. Majjad, B. Doudin, Sub-coercive and multi-level ferroelastic remnant states with resistive readout, Appl. Phys. Lett. 104 (2014) 232905.
[24] Y. Lee, Z.Q. Liu, J.T. Heron, J.D. Clarkson, J. Hong, C. Ko, M.D. Biegalski, U. Aschauer, S.L. Hsu, M.E. Nowakowski, J. Wu, H.M. Christen, S. Salahuddin, J.B. Bokor, N.A. Spaldin, D.G. Schlom, R. Ramesh, Large resistivity modulation in mixed-phase metallic systems, Nat. Commun. 6 (2015) 5959.
[25] L.P. Chen, J. Gao, Reversible in situ modulation of competing phases in manganite/ferroelectrics heterostructures, EPL 93 (2011) 47009.
[26] M.C. Dekker, A.D. Rata, K. Boldyreva, S. Oswald, L. Schultz, K. Dörr, Colossal elastoresistance and strain-dependent magnetization of phase-separated $(Pr_{1-y}La_y)_{0.7}Ca_{0.3}MnO_3$ thin films, Phys. Rev. B 80 (2009) 144402.
[27] M. Zheng, R.K. Zheng, Electric-field-tunable ferroelastic control of nonvolatile resistivity and ferromagnetic switching in multiferroic $La_{0.67}Ca_{0.33}MnO_3/[PbMg_{1/3}Nb_{2/3}O_3]_{0.7}$-$[PbTiO_3]_{0.3}$ heterostructures, Phys. Rev. Appl. 5 (2016) 044002.
[28] B.M. Zhang, C.J. Sun, W.M. Lü, T. Venkatesan, M.G. Han, Y.M. Zhu, J.S. Chen, G.M. Chow, Electric-field-induced strain effects on the magnetization of a $Pr_{0.67}Sr_{0.33}MnO_3$ film, Phys. Rev. B 91 (2015) 174431.
[29] M. Zheng, M.M. Yang, Q.X. Zhu, X. Li, G.Y. Gao, R.K. Zheng, Y. Wang, X.M. Li, X. Shi, H.S. Luo, X.G. Li, Tunable interface strain coupling and its impact on the electronic transport and magnetic properties of $La_{0.5}Ca_{0.5}MnO_3/Pb(In_{1/2}Nb_{1/2})O_3$-$Pb(Mg_{1/3}Nb_{2/3})O_3$-$PbTiO_3$ multiferroic heterostructures, Phys. Rev. B 90 (2014) 224420.
[30] Z.G. Sheng, J. Gao, Y.P. Sun, Coaction of electric field-induced strain and polarization effects in $La_{0.7}Ca_{0.3}MnO_3$/PMN-PT structures, Phys. Rev. B 79 (2009) 174437.
[31] T. Fujiwara, M. Korotin, Spin and orbital ordering of $Nd_{1-x}Sr_xMnO_3$ from LSDA+U calculations, Phys. Rev. B 59 (1999) 9903.
[32] Y. Wakabayashi, D. Bizen, H. Nakao, Y. Murakami, M. Nakamura, Y. Ogimoto, K. Miyano H. Sawa, Novel orbital ordering induced by anisotropic stress in a manganite thin film, Phys. Rev. Lett. 96 (2006) 017202.
[33] M. Nakamura, Y. Ogimoto, H. Tamaru, M. Izumi, K. Miyano, Phase control through anisotropic strain in $Nd_{0.5}Sr_{0.5}MnO_3$ thin films, Appl. Phys. Lett. 86 (2005) 182504.
[34] Y. Ogimoto, M. Nakamura, N. Takubo, H. Tamaru, M. Izumi, K. Miyano, Strain-induced crossover of the metal-insulator transition in perovskite manganites, Phys. Rev. B 71 (2005) 060403(R).
[35] A. Biswas, M. Rajeswari, R.C. Srivastava, T. Venkatesan, R.L. Greene, Q. Lu, A.L. de Lozanne, A.J. Millis, Strain-driven charge-ordered state in $La_{0.67}Ca_{0.33}MnO_3$, Phys. Rev. B. 63 (2001) 184424.
[36] E.R. Buzin, W. Prellier, Ch. Simon, S. Mercone, B. Mercey, B. Raveau, J. Sebek, J. Hejtmanek, Control of the colossal magnetoresistance by strain effect in thin films, Appl. Phys. Lett. 79 (2001) 647.
[37] H. Bai, X.F. Zhou, Y.J. Zhou, X.Z. Chen, Y.F. You, F. Pan, C. Song, Functional antiferromagnets for potential applications on high-density storage and high frequency, J. Appl. Phys. 128 (2020) 210901.
[38] X.Z. Chen, X.F. Zhou, R. Cheng, C. Song, J. Zhang, Y.C. Wu, Y. Ba, H.B. Li, Y.M. Sun, Y.F. You, Y.G. Zhao, F. Pan, Observation of the antiferromagnetic spin Hall effect, Nat. Mater. 18 (2019) 931–935.
[39] H. Yan, Z.X. Feng, S.L. Shang, X.N. Wang, Z.X. Hu, J.H. Wang, Z.W. Zhu, H. Wang, Z.H. Chen, H. Hua, W.K. Lu, J.M. Wang, P.X. Qin, H.X. Guo, X.R. Zhou, Z.G.G. Leng, Z.K. Liu, C.B. Jiang, M. Coey, Z.Q. Liu, A piezoelectric, strain-controlled antiferromagnetic memory insensitive to magnetic fields, Nat. Nanotechnol. 14 (2019) 131–136.
[40] X.N. Wang, Z.X. Feng, P.X. Qin, H. Yan, X.R. Zhou, H.X. Guo, Z.G. Leng, W.Q. Chen, Q.N. Jia, Z.X. Hu, H.J. Wu, X. Zhang, C.B. Jiang, Z.Q. Liu, Integration of the noncollinear antiferromagnetic metal Mn_3Sn onto ferroelectric oxides for electric-field control, Acta Mater 181 (2019) 537–543.
[41] Y. Liu, T.Y. Ma, K.M. Qiao, J. Li, A.D. Xiao, J. Wang, F.X. Hu, B.G. Shen, Strain control of phase transition and magnetocaloric effect in $Nd_{0.5}Sr_{0.5}MnO_3$ thin films, Appl. Phys. Lett. 116 (2020) 082402.
[42] U. Gebhardt, N.V. Kasper, A. Vigliante, P. Wochner, H. Dosch, F.S. Razavi, H.U. Habermeier, Formation and thickness evolution of periodic twin domains in manganite films grown on $SrTiO_3$(001) substrates, Phys. Rev. Lett. 98 (2007) 096101.
[43] Y.H. Chen, T.B. Wu, Thickness dependent transport properties and percolative phase separation in polycrystalline manganite thin films, Appl. Phys. Lett. 93 (2008) 224104.
[44] I.G. Deac, J.F. Mitchell, P. Schiffer, Phase separation and low-field bulk magnetic properties of $Pr_{0.7}Ca_{0.3}MnO_3$, Phys. Rev. B 63 (2001) 172408.

[45] D. Niebieskikwiat, R.D. Sánchez, Pinning of elastic ferromagnetic/antiferromagnetic interfaces in phase-separated manganites, J. Phys.: Condens Matter 24 (2012) 436001.
[46] A. Tebano, C. Aruta, S. Sanna, P.G. Medaglia, G. Balestrino, Evidence of orbital reconstruction at interfaces in ultrathin $La_{0.67}Sr_{0.33}MnO_3$ films, Phys. Rev. Lett. 100 (2008) 137401.
[47] C. Aruta, G. Ghiringhelli, V. Bisogni, L. Braicovich, N.B. Brookes, A. Tebano, G. Balestrino, Orbital occupation, atomic moments, and magnetic ordering at interfaces of manganite thin films, Phys. Rev. B 80 (2009) 014431.
[48] I-Ting Chiu, A.M. Kane, R.V. Chopdekar, P. Lyu, A. Mehta, C.M. Rouleau, A.T. N'Diayec, E. Arenholz, Y. Takamura, Phase transitions and magnetic domain coexistence in $Nd_{0.5}Sr_{0.5}MnO_3$ thin films, J Magn. Magn. Mater. 498 (2020) 166116.
[49] J. López, P.N. Lisboa-Filho, W.A.C. Passos, W.A. Ortiz, F.M. Araujo-Moreira, Magnetic relaxation behavior in $La_{0.5}Ca_{0.5}MnO_3$ and $Nd_{0.5}Sr_{0.5}MnO_3$, Phys. Rev B 63 (2001) 224422.
[50] W. Eerenstein, M. Wiora, J.L. Prieto, J.F. Scott, N.D. Mathur, Giant sharp and persistent converse magnetoelectric effects in multiferroic epitaxial heterostructures, Nat. Mater. 6 (2007) 348–351.
[51] Y.J. Yang, M.M. Yang, Z.L. Luo, H.L. Huang, H.B. Wang, J. Bao, C.S. Hu, G.Q. Pan, Y.P. Yao, Y.K. Liu, X.G. Li, S. Zhang, Y.G. Zhao, C. Gao, Large anisotropic remnant magnetization tunability in (011)-$La_{2/3}Sr_{1/3}MnO_3$/0.7$Pb(Mg_{2/3}Nb_{1/3})O_3$-0.3$PbTiO_3$ multiferroic epitaxial heterostructures, Appl. Phys. Lett. 100 (2012) 043506.
[52] R.O. Cherifi, V. Ivanovskaya, L.C. Phillips, A. Zobelli, I.C. Infante, E. Jacquet1, V. Garcia, S. Fusil1, P.R. Briddon, N. Guiblin, A. Mougin, A.A. Ünal, F. Kronast, S. Valencia, B. Dkhil, A. Barthélémy, M. Bibes, Electric-field control of magnetic order above room temperature, Nat. Mater. 13 (2014) 345–351.
[53] T. Wu, P. Zhao, M.Q. Bao, A. Bur, J.L. Hocke, K. Wong, K.P. Mohanchandra, C.S. Lynch, G.P. Carman, Domain engineered switchable strain states in ferroelectric (011) $[Pb(Mg_{1/3}Nb_{2/3})O3](1-x)$-$[PbTiO_3]x$ (PMN-PT, $x\approx0.32$) single crystals, J. Appl. Phys 109 (2010) 124101.
[54] B.A. Strukov, A.P. Levanyuk, in: Ferroelectric Phenomena in Crystals, Springer, New York, 1998, p. 35.
[55] I.W. Chen, Y. Wang, A domain wall model for relaxor ferroelectrics, Ferroelectrics 206 (1998) 245–263.
[56] T. Jiang, S.W. Yang, Y.K. Liu, Y.W. Yin, S.N. Dong, W.B. Zhao, X.G. Li, Coaction and distinguishment of converse piezoelectric and field effects in $La_{0.7}Ca_{0.3}MnO_3/SrTiO_3$/0.68$Pb(Mg_{1/3}Nb_{2/3})O_3-0.32PbTiO_3$ heterostructures, Appl. Phys. Lett. 103 (2013) 053504.
[57] E.J. Guo, J. Gao, H.B. Lu, Coaction of strain and polarization effects on tuning the photoinduced resistance changes in $La_{0.9}Sr_{0.1}MnO_3$ films, EPL 95 (2011) 47006.
[58] G. Vinai, F. Motti, V. Bonanni, A.Yu. Petrov, S. Benedetti, C. Rinaldi, M. Stella, D. Cassese, S. Prato, M. Cantoni, G. Rossi, G. Panaccione, P. Torelli, Reversible modification of ferromagnetism through electrically controlled morphology, Adv. Electron. Mater. 5 (2019) 1900150.
[59] Z.Q. Liu, J.H. Liu, M.D. Biegalski, J.M. Hu, S.L. Shang, Y. Ji, J.M. Wang, S.L. Hsu, A.T. Wong, M.J. Cordill, B. Gludovatz, C. Marker, H. Yan, Z.X. Feng, L. You, M.W. Lin, T.Z. Ward, Z.K. Liu, C.B. Jiang, L.Q. Chen, R.O. Ritchie, H.M. Christen, R. Ramesh, Electrically reversible cracks in an intermetallic film controlled by an electric field, Nat. Commun. 9 (2018) 41.
[60] M. Liu, B.M. Howe, L. Grazulis, K. Mahalingam, T.X. Nan, N.X. Sun, G.J. Brown, Voltage-impulse-induced non-volatile ferroelastic switching of ferromagnetic resonance for reconfigurable magnetoelectric microwave devices, Adv. Mater. 25 (2013) 4886–4892.
[61] Y. Ba, Y. Liu, P.S. Li, L. Wu, J. Unguris, D.T. Pierce, D. Yang, C. Feng, Y.K. Zhang, H. Wu, D.L. Li, Y.S. Chang, J.X. Zhang, X.F. Han, J.W. Cai, C.W. Nan, Y.G. Zhao, Spatially resolved electric-field manipulation of magnetism for CoFeB mesoscopic discs on ferroelectrics, Adv. Funct. Mater. 28 (2018) 1706448.
[62] X.E. Zhao, R.C. Peng, Z.Q. Hu, T.N. Yang, W.X. Hou, Y.Q. Zhou, T. Li, Q. Du, Y.X. Cheng, J.G. Wu, Z.G. Wang, Z.Y. Zhou, L.Q. Chen, M. Liu, Shear-strain-induced over 90° rotation of local magnetization in FeCoSiB/PMN-PT (011) multiferroic heterostructures, Acta Mater 199 (2020) 495–503.